THE ASTROPHYSICAL JOURNAL, 366:38–49, 1991 January 1

GALAXY VELOCITY DISPERSIONS USING A CROSS-CORRELATION METHOD[1]

CRISTINA DALLE ORE, S. M. FABER, J. JESÚS AND ROLAND STOUGHTON
University of California Observatories/Lick Observatory, Board of Studies in Astronomy and Astrophysics, University of California, Santa Cruz

AND

DAVID BURSTEIN
Department of Physics and Astronomy, Arizona State University, Tempe
Received 1990 January 10; accepted 1990 June 27

ABSTRACT

Lick image-dissector scanner spectra obtained from 1972 to 1984 have been used to derive central velocity dispersions for over 350 elliptical galaxies, as published in an earlier paper. This paper details the cross-correlation method used and tabulates central velocity dispersions for 79 additional early-type galaxies not included in that earlier work. The special problems of using the cross-correlation method as applied to IDS data are addressed, and various tests of the effects of random and systematic errors are made to establish the accuracy of the results. A significant difference is described between the present cross-correlation technique and the method as originally developed by Tonry and Davis.

Subject headings: galaxies: internal motions — numerical methods

I. INTRODUCTION

From 1972 to 1984, we pursued a steady effort at Lick Observatory to accumulate spectra of the nuclei of early-type galaxies with the goal of measuring line strengths and velocity dispersions. The line-strength work is still in progress and will be reported separately. Most of the velocity dispersions on ellipticals appeared in the E-galaxy compendium by Davies *et al.* (1987), which merged Lick dispersions with results from Kitt Peak, Las Campanas, and the Anglo-Australian Telescope. However, an additional 79 nonelliptical galaxies were not included in that paper. We present these measurements here and provide details on the cross-correlation method used to determine the dispersions.

Several methods have been used in the past to measure velocity dispersions. Minkowski (1962) pioneered the field and broadened stellar template spectra photographically by exposing through semitransparent slit jaws or by smearing spectra in the darkroom. With the advent of computers, it was no longer necessary to produce broadened stellar templates photographically; they could be computed analytically by convolution with Gaussians of known widths. This technique was introduced by Richstone and Sargent (1972), Morton and collaborators (1973, 1976), and by Williams (1976). However, comparison between galaxy and broadened template was generally still made visually and involved subjective judgment.

Faber and Jackson (1976) attempted to develop a more objective criterion based on the width of the power spectrum. Their method made use of the convolution theorem for Fourier transforms: in Fourier space, the observed galaxy spectrum is the product of the intrinsic (unbroadened) galaxy spectrum multiplied by the velocity distribution function (usually assumed to be Gaussian). The basic principles were discussed by Brault and White (1971) and Simkin (1974), and the method was used to measure velocity dispersions for globular clusters and galaxies by Illingworth (1976), Illingworth and Freeman (1974), and Simkin (1974).

Faber and Jackson compared results from the power-spectrum and visual methods and found good agreement at the 5% level. However, they noted a problem caused by nonwhite noise in the Lick image-dissector scanner (IDS) detector. Let

$$o(\ln \lambda) = \text{observed spectrum of galaxy},$$

$$g(\ln \lambda) = \text{true spectrum of galaxy},$$

$$d(\ln \lambda) = \text{noise in observed galaxy spectrum},$$

and let $O(k)$, $G(k)$, and $D(k)$ be the corresponding Fourier transforms. In the power domain,

$$|O|^2 = |G|^2 + |D|^2 , \tag{1}$$

so that noise in this domain does not average to zero but provides a net bias that must be subtracted off. Faber and Jackson found that the IDS noise was large and variable and peaked at the frequencies of most interest for velocity dispersions. Even careful attempts to subtract it off yielded dubious results, and in the end, they gave their visual estimates higher weight.

Schechter (in Sargent *et al.* 1977) pioneered the form of the Fourier method that has now become standard. Schechter observed that one could avoid the net bias that plagues the power-spectrum method by fitting to the phase of $O(k)$ as well as to the modulus. Since the noise has random phase, it averages to zero in the real and imaginary components separately, and there is no need to subtract it off. However, the noise *does* affect the weights one should apply in fitting $O(k)$ to the model in frequency space. Thus some knowledge of the noise is still required, but the accuracy needed is reduced. The issue of the noise is clearly a key factor in deriving velocity dispersions and has in fact led us to our final choice of the cross-correlation method over the more conventional Fourier approach. However, before discussing our procedures, we first describe the image-dissector scanner and the data from it so that the reader can better understand the nature of the noise and its effects.

[1] UCO/Lick Observatory Bulletin No. 1171.

II. OBSERVATIONAL DATA AND NOISE

The observations were taken from 1972 to 1985 with the Robinson-Wampler image dissector scanner (Robinson and Wampler 1972) at the 3.0 m Shane Telescope of the Lick Observatory. Details of the observing technique and the data are given in Faber *et al.* (1985) and Burstein *et al.* (1984). The original spectra cover ~4100 Å–6200 Å at a dispersion of 1.25 Å per channel. The resolution is typically 10 Å FWHM but varied slightly from run to run. Resolution changes were monitored nightly by observing K-giant standard stars. Many other stars of a wide variety of spectral types were also observed.

Pixel-to-pixel response variations were removed by dividing by an internal quartz-iodide continuum lamp. No absolute flux standards were observed, and, as a result, the reduced spectra contain irregular large-scale undulations that must be removed before the dispersions can be measured. Various detrending approaches were tried and are discussed below.

Wavelength calibrations were obtained from observations of He, Ne, Hg, and Cd comparison lamps. A good calibration required a long exposure to bring in the faint lines, during which time the bright lines were severely over-exposed. This over-exposure took a long time to decay because of the persistence of the intensifier phosphors in the IDS. The comparison lamps were consequently observed only at the beginning and end of each night.

The wavelength scales of the individual scans are somewhat uncertain owing to flexure in the grating tray and distortions in the dissector electron optics due to variable stray magnetic fields. Changes in the dome azimuth and spectrograph orientation produced shifts in the wavelength scale of up to three channels. However, these were not large enough to degrade the velocity dispersions, as shown below under tests.

The spectrograph had two apertures separated by either 21″ or 35″ on the sky. These produced two parallel spectra on the detector, one for the object, and one for the sky. During an exposure, the object was passed back and forth between the two apertures in such a way as to equalize the time spent in both. Appropriate subtraction of the data yielded the spectrum of the object alone in each slit, called "left" and "right." The "sum" of the two slits is independent to first order of small changes in the night-sky spectrum due to passing clouds and is therefore more reliable than right or left separately.

The entrance apertures on the sky measured 1.″5 × 4.″0. In wavelength units, the slit width of 1.″5 projects to about 4.1 Å. This is small enough compared to the total FWHM of 10 Å that the net spectral resolution is determined essentially by the detector resolution. Changes in the seeing thus had no observable effect on the linewidths.

The IDS consisted of a chain of three image-intensifier tubes followed by an image dissector. The finite time response of the phosphors in the intensifier chain produced an output burst of light with a time decay of ~100 ms. During that time, the image dissector scanned over both the object and the sky spectra at least once, and the gain was such that typically 10 or more output photons were detected per input photon. Each input photon thus resulted in a burst of roughly 10 output photons, with width equal to the resolution of the intensifier-dissector chain, i.e., ~10 Å.

The output noise of such a device has two components. The first is a nonwhite component due to the shot noise of the incoming photons. Since each input photon is sensed over several adjacent channels, this input noise is correlated from channel to channel and peaks at low frequencies. The second component is due to the shot noise of the amplification process, which is just $\sqrt{N}$ of the total number of output photons. This second noise is random from channel to channel and is therefore white. The relative amplitude of the second component is lower than that of the first because the number of output photons exceeds the number of input photons. In fact, the difference in the two noise amplitudes is a measure of the gain of the intensifier chain. It is this gain that caused trouble for the power-spectrum method of Faber and Jackson (1976). It varies from run to run and even within a single night, causing the net power spectrum of the noise to vary.

Examples of typical IDS power spectra for a star and galaxy are reproduced from Faber and Jackson in Figure 1. The noise spectra (dotted lines) were estimated by dividing the data from the left and right slits. The two noise components are separately visible as the central hump and sloping shoulders in the noise profiles (the original white noise at high frequencies is "reddened" slightly when the raw data are interpolated onto a wavelength scale). Comparison of the spectra provides some indication of the degree of variability of the noise.

III. THE CROSS-CORRELATION METHOD

The cross-correlation method which we use here was introduced for velocity dispersions by Tonry and Davis (TD 1979). In this method, one cross-correlates the galaxy spectrum against an essentially noiseless stellar template. The width of the cross-correlation peak is a measure of the width of the galaxy features, which can be seen as follows. Let $t(\ln \lambda)$ and $v(\ln \lambda)$ be the template spectrum and the velocity broadening function, respectively. If v is a Gaussian, and t is a good match to the unbroadened galaxy spectrum, we have

$$g(\ln \lambda) = t(\ln \lambda) * v(\ln \lambda)$$
$$= t(\ln \lambda) * C \exp\left[\frac{-(\ln \lambda)^2 c^2}{2\sigma^2}\right], \quad (2)$$

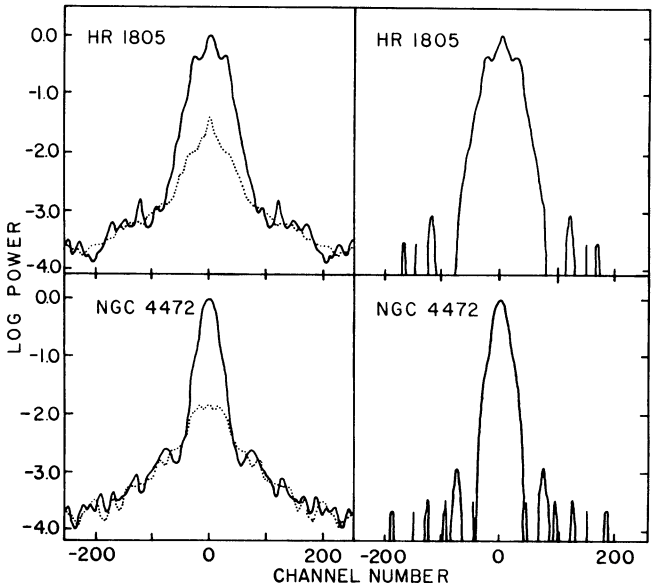

FIG. 1.—From Faber and Jackson (1976). (*Left*) sample IDS power spectra of a star, galaxy, and noise (*dotted line*). Each channel in frequency space represents one cycle per $\Delta \ln \lambda = 0.125$. (*Right*) power spectra of signal after noise subtraction.

where σ is the velocity dispersion, c is the velocity of light, C is a normalizing constant, and the asterisk denotes convolution. (Note that, by writing g and t as functions in $\ln \lambda$ rather than λ, we are able to represent v as a Gaussian of constant width independent of wavelength.)

Now define the lag, d, in units of $\Delta \ln \lambda$/channel, and let $[a \times b \mid d]$ denote the cross correlation of a and b evaluated at lag d. Then, using equation (2) in integral form, we have

$$\begin{aligned}[t \times g \mid d] &= \int_{-\infty}^{\infty} t(p)dp \int_{-\infty}^{\infty} v(q)t(p + d - q)dq \\ &= \int_{-\infty}^{\infty} v(q)dq \int_{-\infty}^{\infty} t(p)t(p + d - q)dp \\ &= \int_{-\infty}^{\infty} v(q)[t \times t \mid d - q]dq \\ &= [(t \times t) * v \mid] . \end{aligned} \tag{3}$$

Thus, in the cross-correlation of g with t, velocity broadening in the galaxy acts like a convolution of the template autocorrelation function with v. In the case of Gaussian broadening, the width of $t \times g$ thus depends directly on σ and can be used as an estimator of it. In the present work, we convolve $t \times g$ by Gaussians of various widths and choose that value of σ that matches the observed FWHM of $t \times g$ equation (3) is more general than this, however, and can be used to test for broadening functions of any shape, asymmetric as well as symmetric. In practice, however, we find that departures from asymmetry in the present data are not large and would require much higher S/N observations to determine reliably. Examples of $t \times g$ and the high degree of symmetry are shown in Figures 4 and 7 below.

At this point, we explain why we selected the cross-correlation technique for the Lick IDS data over the more standard Fourier approach. In principle there is no difference in accuracy between the two methods: as long as the template width is reasonably small compared to the width of the velocity-broadening function, the accuracy in σ is the same either way, as can be verified from a direct calculation of S/N. However, since the IDS noise is not white, some knowledge of its behavior with frequency is still required to determine the optimum fitting weights in frequency space with the Fourier method. This poses a difficult requirement because of the fact that the power spectrum of IDS noise is variable on fairly short time scales (hours). Hence, care would have to be taken to monitor the variations and to update the optimum weights versus frequency.

We have chosen the cross-correlation method instead because of its complete insensitivity to nonwhite noise. In the cross-correlation domain, nonwhite Gaussian noise shows up simply as smoothed *random* noise, with amplitude and phase both independent of lag. In determining the width of the cross-correlation peak, all channels around the peak can therefore be assigned the same error, i.e., the weighting scheme is independent of the noise power spectrum. This simplicity is an appealing advantage in dealing with nonwhite noise.

Before giving details, we highlight two differences between our treatment and that of Tonry and Davis, whose approach we generally follow. Tonry and Davis smoothed and detrended their data before cross-correlation using a combination low- and high-pass filter in the Fourier domain. We have not presmoothed our spectra since we believe that smoothing has no positive value and even degrades the accuracy in σ if the smoothing window is large. The accuracy in σ clearly depends on the accuracy of the width of the cross-correlation peak, W. It can be shown that the error in W scales roughly as

$$\frac{\Delta W}{W} \sim \frac{1}{\sqrt{N_c}} \frac{\Delta y}{y} , \tag{4}$$

where y is the cross-correlation versus lag, $\Delta y/y$ is the typical uncertainty of the cross-correlation (per channel) near the peak, and N_c is the number of statistically independent data channels in the peak. From equation (3), we have seen that smoothing the input galaxy spectrum is simply equivalent to smoothing the cross-correlation function. Assume then that the smoothing width in channels, N_s, is small compared to W. The noise, $\Delta y/y$, is then reduced by $\sqrt{(N_s)}$, but the number of independent channels, N_c, is also reduced by N_s, and the net error in W is therefore unchanged. On the other hand, if N_s is large compared to W, the effect is actually to degrade W, as the number of statistically independent channels approaches unity, too small to measure a width. We conclude that presmoothing the galaxy data does not increase the accuracy of measured velocity dispersions and may actually degrade it. Not surprisingly, a similar calculation shows a similar lack of efficiency for the Fourier method, too.

We have also taken a different approach from TD with regard to detrending. Briefly, the cross-correlation functions for stellar and galaxy spectra are highly symmetric and consist of a central narrow peak (caused by individual absorption lines) superposed on a broader baseline (caused by blends and large-scale trends; see Fig. 4 below). The width of the narrow peak is the sensitive measure of the velocity dispersion, but this unfortunately interacts with the shape and amplitude of the baseline, which in turn can depend on the exact nature of the spectrum and the precise method of detrending used (see below). We at first tried to control baseline shape via an appropriate choice of detrending method. Numerous attempts proved unsuccessful, however, and we instead found it necessary to fit and remove the baseline directly from the cross-correlation function itself. Peak width was then defined as the FWHM of the central peak *after baseline subtraction*, which proved to be an accurate and stable measure of W. With control over the baseline thus improved, the precise method of detrending became unimportant, and we found it adequate simply to flatten the data with a fifth-order polynomial, as opposed to the more elaborate high-pass Fourier filter used by TD.

How to remove the baseline accurately occupied most of our efforts in perfecting the cross-correlation method. This and the sensitivity of baseline shape to various types of detrending are described in detail in § VI below.

IV. PREPARATION OF SPECTRA

During data reduction, all three spectra—left, right, and sum—were reduced separately for velocity dispersion. On nearly all nights, there were enough standard stars that the night could be reduced as an independent unit. On each such night, we grouped the data into three categories; one K giant with excellent S/N selected as TEMPLATE, additional K giant STARS as standards, and program GALAXIES.

Spectra were first mapped into logarithmic wavelength bins of width 60 km s^{-1} ($\Delta \ln \lambda = 2.0 \times 10^{-4}$). The next step was a trial cross-correlation with the template to check whether the

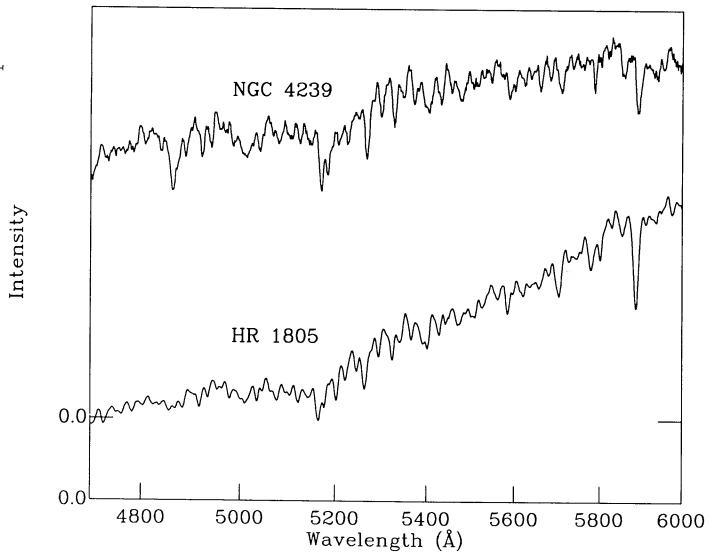

FIG. 2a

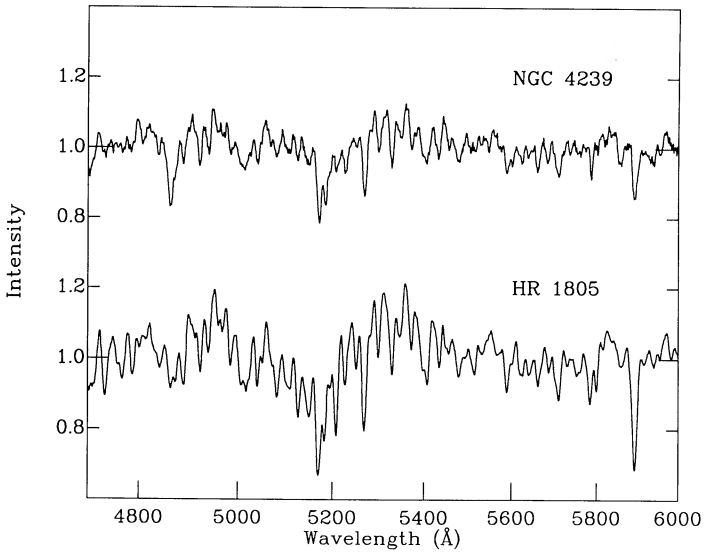

FIG. 2b

FIG. 2.—(*a*) Sample raw spectra of galaxy and K-giant star after division by quartz-iodide lamp. (*b*) Same, after flattening by a fifth-order polynomial.

peak was shifted with respect to zero lag. Such a shift could be due either to an error in the assumed initial wavelength (due to uncertainties in the wavelength scale) or to an error in the assumed redshift of the object (taken from the literature). We assumed that all shifts less than six channels were due to wavelength errors and corrected the wavelength scale accordingly. Shifts greater than 6 channels were ascribed to redshift, which we redetermined assuming that our wavelength scale was correct. This procedure introduced a scale error, or stretch, of at most 2.5 channels from one end of the spectrum to the other. The net effect of such an error on the velocity dispersions is examined below under Tests.

The spectra were then detrended by dividing by a fifth-order polynomial, normalized to unity in the continuum, and reduced to zero mean. Alternative detrending schemes are described below under tests. Figure 2 shows typical star and galaxy spectra before and after detrending.

Owing to clouds and/or instrument flexure during an observation, galaxy spectra sometimes showed poor sky subtraction in the night-sky lines, especially the right or left separately. Since the sum was usually unaffected, we spliced good regions from it into the left and right spectra when necessary. In cases of severe cloud where the sum was also corrupted, and for galaxies with intrinsic line emission, we substituted sections from a standard galaxy spectrum of comparable line strength and broadening and good S/N. Figure 3 shows some typical cases. This procedure was quite successful, based on tests with nonemission galaxies. We went to the effort of using realistic spectral splices after tests using straight-line interpolation proved unsatisfactory (see Fig. 3).

V. MEASUREMENT OF THE VELOCITY DISPERSION

After the TEMPLATE and GALAXY had been prepared as above, the two spectra were cross-correlated. The region used for cross-correlation was 4900–5800 Å. This choice excluded Hβ, which is variable due to star formation and emission, and Na D, which is near the end of the spectrum, in a region of changing spectral resolution. Sample cross-correlations are shown in Figure 4*a* for a template standard star broadened by different amounts. Flattening by a low-order polynomial, as here, leaves many blended features in the spectrum with widths of order 20–40 channels, and these show up in the cross-correlation as a broad *hump*, or pedestal, upon which the narrow peak due to single lines is superposed. This is the baseline effect referred to above in § III. Note that polynomial detrending leaves a *positive hump* in the baseline, whereas a high-pass Fourier filter method, such as that used by Tonry and Davis, leaves a *negative valley*. Such valleys may be seen in Figures 7–9 of TD and also in Figure 6 below, where various Fourier methods are intercompared. We have further observed that changes in spectral type and details of the flattening process can affect the relative importance of the narrow and broad-line spectral features and thus, the relative amplitudes and shape of the baseline versus the central peak. After numer-

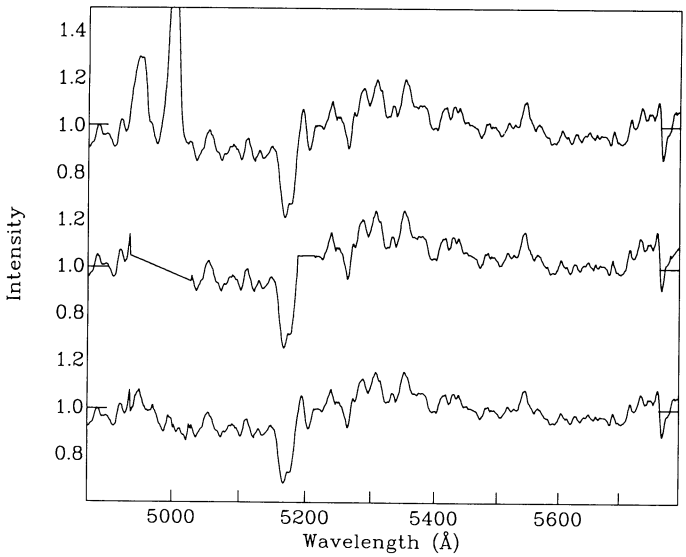

FIG. 3.—Spectra of NGC 1052 illustrating removal of emission lines. (*Top*) original spectrum. (*Middle*) linear interpolation. This technique proved to be unsatisfactory, based on tests with nonemission spectra. (*Bottom*) spliced-in sections of a standard galaxy of similar line-strength and velocity dispersion. Residual weak N I emission at 5199 Å does not affect the results appreciably.

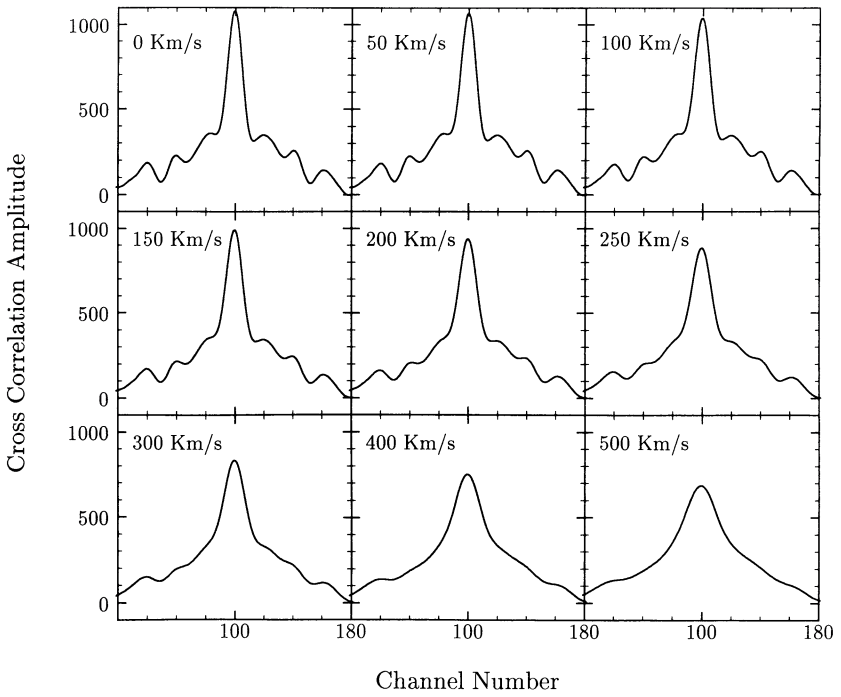

FIG. 4*a*

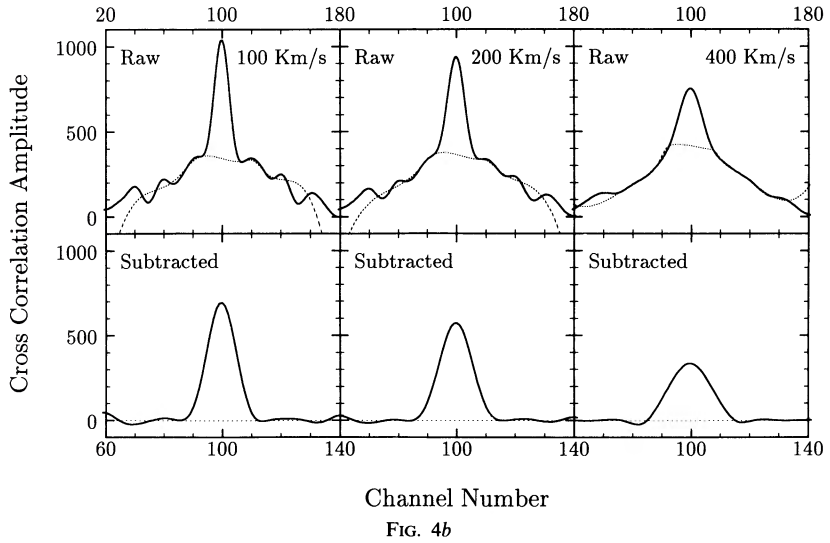

FIG. 4*b*

FIG. 4.—(*a*) Raw cross-correlations of a template K giant with a K-giant standard star broadened by various amounts. Each channel is 60 km s^{-1} ($\Delta \ln \lambda = 2.0 \times 10^{-4}$). Note the broad baseline hump caused by blends and large-scale features. Such a hump results from polynomial detrending. (*b*) Sample spline baseline fits to a broadened standard star. (*Top*) original data. (*Bottom*) after baseline subtraction. (*c*) Same for sample galaxies. The derived dispersions for the galaxies are indicated.

ous unsuccessful attempts at trying to control the shape of the baseline via detrending, we finally decided to fit and remove it from the cross-correlation function directly.

According to equation (3), the series of panels in Figure 4*a* represents convolution of the zero-velocity cross-correlation at upper left with broadening functions of successively greater width. As the broadening is increased, it is seen that the central narrow peak, which carries virtually all of the information about the velocity dispersion, tends to become blended with the shoulders of the baseline pedestal and lose its separate identity. The challenge is to fit the baseline in such a way as to be insensitive to changes in spectral type, detrending, and noise and also without distorting the intrinsic shape of the central peak. In particular, the fitting method must yield consistent peak widths for all standard stars independent of spectral type. The method finally adopted utilized a spline fit to the wings of the pedestal, which was then subtracted off (see tests for further details). Figures 4*b* and 4*c* show examples of the spline fit and the central peak after subtraction for several stars and galaxies. The final cross-correlation width was defined to be the FWHM of the peak after subtraction.

In addition to the program galaxies, cross-correlation widths were measured for each night's standard K giants, broadened by Gaussians of different σ. The resultant width-

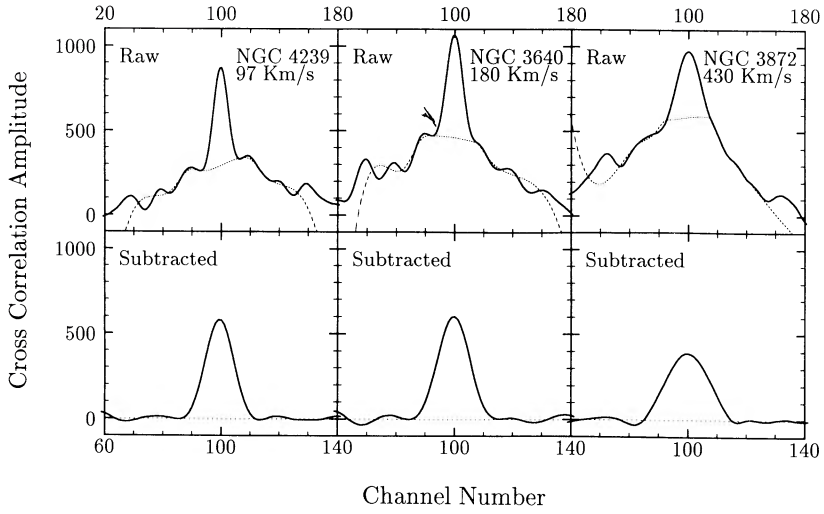

FIG. 4c

versus-σ curve provided a calibration from which σ for the galaxies could be read off. Right, left, and sum were calibrated separately for each night. A sample calibration curve for one night (using sums) is shown in Figure 5, illustrating typical agreement among the standard stars. The adopted curve was the average of all curves except that of the template against itself. The template was not used because noise in an *auto*correlation function biases the central peak too high, making it appear too narrow.

VI. TESTS

a) Baseline Removal

As noted in § III, it is the narrow central peak of the cross-correlation function that carries the main information about the velocity broadening. The broad baseline on which this peak is superposed is due to the presence of blends in the spectrum with a width of 20–40 Å. These blends are intrinsic to the spectrum and cannot be circumvented by observing at higher dispersion.

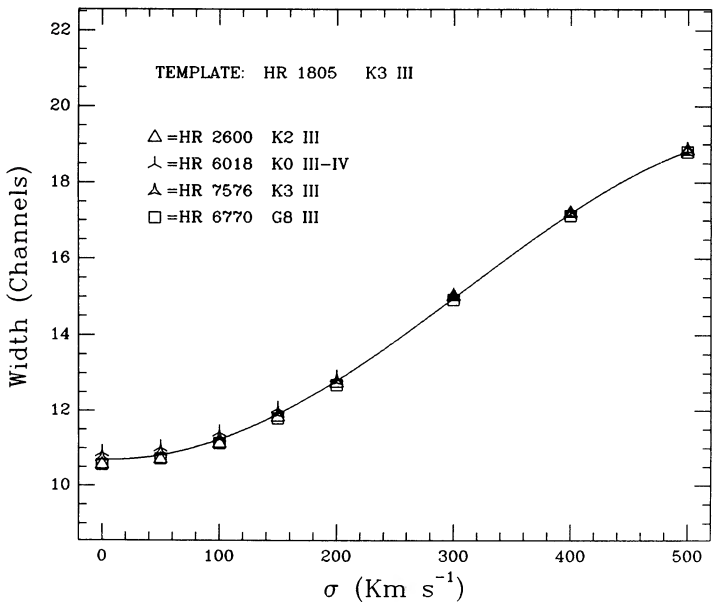

FIG. 5.—A calibration curve of W vs. σ for a typical night. The ordinate is the FWHM of the cross-correlation after baseline subtraction.

If possible, we would like to remove these blends by filtering or flattening the spectra so as to preserve only the narrow features. However, the unwanted blends are not very much broader than the narrow features—the difference is only a factor of 2 or so. Experience shows that this makes their removal essentially impossible. Polynomial detrending is unfeasible, as the degree of polynomial required is very high and the fit becomes unstable. We also tested several high-pass Fourier filters in the spirit of Tonry and Davis, examples of which are shown in Figure 6. These tests started with spectra flattened by fifth-order polynomials, from which the same spectra, smoothed by boxcars, Gaussians, and sinc-functions of various widths, were subtracted. Negative wings or valleys typically result of the sort already noted in the cross-correlations of Tonry and Davis. The valleys produced by high-pass filtering contrast with the positive hump that comes from polynomial smoothing.

Peak width (measured above zero) in Figure 6 correlates exactly with peak height, and thus with the shape of the baseline. FWHM's range from 8.2 channels for the lowest peak (box 50) to 12.5 channels for the highest peak (sinc 17.59). The range in this quantity is not what matters, however, but rather the *stability* of the FWHM for a given detrending method. As Figure 6 graphically shows, this in turn depends on the stability of the baseline shape that can be achieved for that method. Experimentally we found that, whatever flattening method was employed, we encountered variations that were typically like those shown by the lower right four panels in Figure 6 (medium and wide Gaussians and sincs). The total range in FWHM among these four panels is 10.4–11.4 channels. Consulting the calibration in Figure 5, we see that this corresponds to a range in σ of 150 km s^{-1} for $\sigma \leq 100$ km s^{-1} and 50 km s^{-1} for $\sigma \approx 250$ km s^{-1}. These errors are unacceptable.

The good news in Figure 6 is that the height (and width) of the central peak measured above the *local* baseline is a much more stable quantity than the height (or width) above zero. Subtracting the local baselines just by eye, we find that all of the panels in Figure 6 now have peak widths in the range 10.2–10.7 channels, and most are clustered near 10.4 channels.

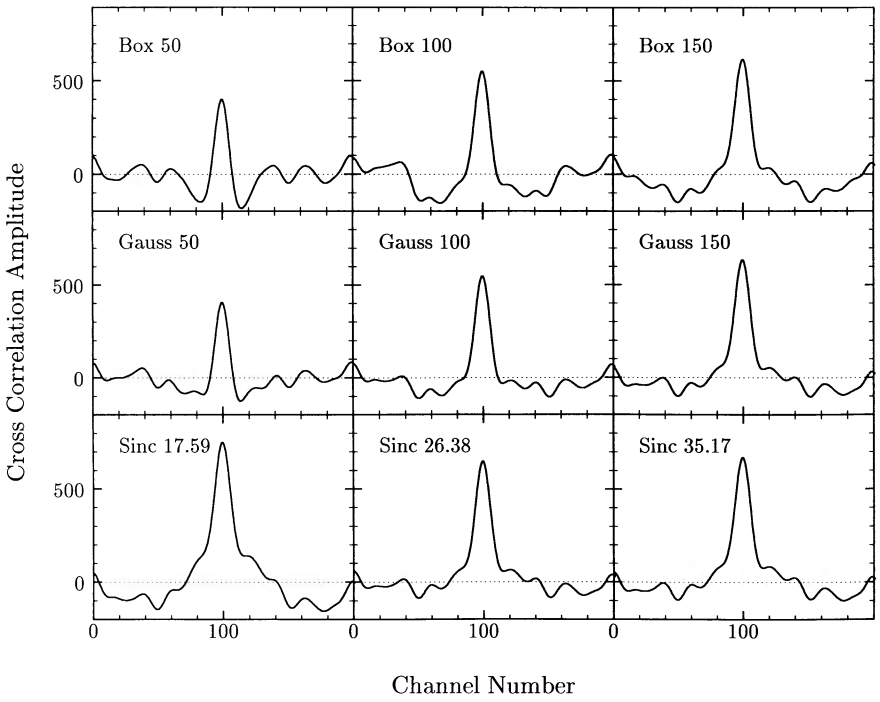

FIG. 6.—The effect on the cross-correlation function of a K-giant star produced by detrending by three types of Fourier filters. In all cases, the logarithmically binned spectrum is smoothed by a function of the indicated form and width, and this smoothed spectrum is subtracted, leaving behind the high frequencies. The indicated widths are in channels of the logarithmically binned spectra, i.e., 60 km s^{-1} per channel. *Top*: Box-car smoothing. *Middle*: Gaussian smoothing with indicated FWHM. *Bottom*: Smoothing by a sinc function, with indicated width equal to the distance from zero to the first minimum. Smoothing by the last function and subtraction corresponds to filtering by a simple high-pass boxcar in Fourier space, the method used by TD. The Fourier forms for the top two filters are more complicated and are given by $(1 - F[v])$, where $F(v)$ is the Fourier transform of the smoothing function. Note the negative wings (valleys) introduced by all of these Fourier filters, in contrast to the hump introduced by polynomial detrending, seen in Figs. 4 and 7.

Broadening information thus seems to be preserved in the cross-correlation function, but, to get at it, we must evidently extract the baseline very accurately.

These results led us to concentrate on fitting and subtracting the baseline from the cross-correlation function itself. Several methods were tried, all of which attempted to fit a smooth curve through the pedestal wings. Polynomials of all orders proved unsatisfactory, as they did not follow the baseline closely enough (see Fig. 7). After extensive experimentation, we adopted a spline smoothing function (ICSSCU in the IBM Mathematical Subroutine Library). The channel intervals $(-50, -16)$ and $(+16, +50)$ were each divided into three equal segments, and the means of the cross correlation function were computed in each segment. These provided six data points for the spline smoothing function. In addition, the values of the cross correlation function near the base on either side of the narrow peak in channels $+16$ and -16 were added, and these points were each duplicated, making 10 data points in all. The weights of the duplicated points were each ten times the weights of the other points, which forced the smoothing function to go very closely through the base of the narrow peak. Duplicating the points made it possible for the spline fit to "turn the corner" rapidly near the base of the narrow peak. The routine ICSSCU fits that natural spline that has smallest rms second derivative and weighted rms residual less than some specified smoothing parameter, S. We chose $S = 5$, which forced a fairly tight fit. This rather complicated recipe yielded reproducible results on different standard stars and also on noisy galaxy spectra. Examples of baseline fitting and subtraction on four stars and galaxies are shown in Figure 7.

It is curious that our spectra required extreme care in treating the baseline whereas Tonry and Davis did not report the same problem. This is especially puzzling in view of their adopted definition of peak width as simply FWHM above zero-level, with no correction whatsoever for baseline. This definition depends on directly the relative heights of the central peak and valley and thus, in our experience, should vary with spectral type. Although we do not understand this difference, we have described the baseline problem and our treatment of it in some detail for the benefit of others who may discover the same sensitivity in their own data.

b) Wavelength Calibration Errors

The logarithmically binned spectra suffer possible accordion errors of up to 2.5 channels owing to stray magnetic fields and errors in the initial wavelengths. A stretching or compression of the wavelength scale causes an error in the peak width. We checked this effect by introducing an artificial scale error of a few channels at one end of the spectrum with respect to the other. A stretch or compression of 10 channels corresponds to an error of ~ 100 km s^{-1} at small dispersions and 40 km s^{-1} at larger dispersions. Since the maximum scale error is less than a quarter of this, the resultant error in the dispersions is small compared to photon statistics.

c) Choice of Standard Stars

K giants were chosen as standard stars whenever possible since they contribute the majority of the light of early-type galaxies in this spectral region. To investigate the error introduced by the mixture of stellar types in the galaxy and by the occasional substitution of other stellar types for K giants, we computed calibration curves for a variety of stars between

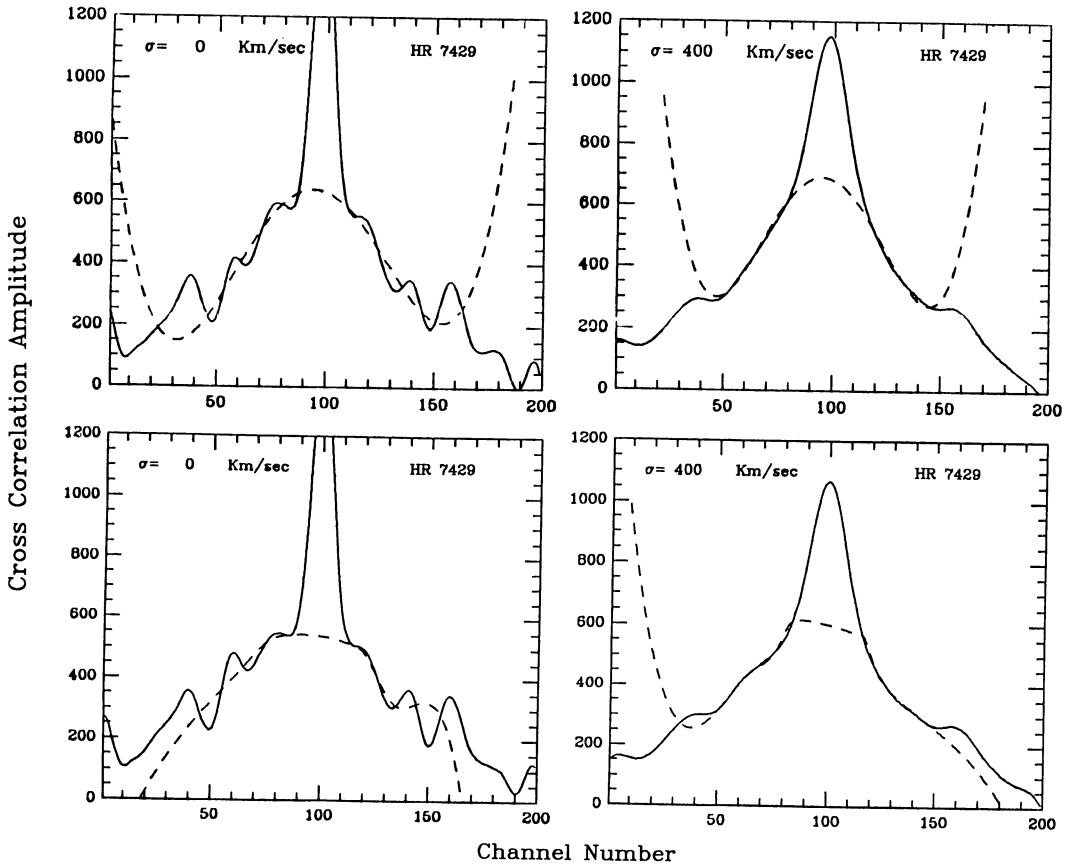

FIG. 7a

FIG. 7.—(*a*)–(*c*) Examples of baseline fitting to stars and galaxies. In each panel sixth-order polynomials are fitted on top. Note the frequent lack of a good fit to the baseline near the base of the central peak. The adopted spline fits are shown at bottom. The good fit at the base in this case was accomplished by placing high-weight knots in channels ±16 from the peak.

spectral types F4 and K4 of different luminosity classes. Figure 8 shows the difference in the width of the calibration curve at zero broadening for the test stars versus the template (always a K-giant). Dwarfs are open circles, giants are solid dots. There is a slight systematic offset due to noise bias in the template correlated against itself, but otherwise no systematic variation with spectral type. In agreement with previous studies, we conclude that errors in the velocity dispersion due to spectral mismatch are negligibly small.

VII. RESULTS

The individual measurements are listed in Table 1, with right, left, and sum indicated separately. The mean values in the last column are averages of the sums, with the colons given half weight. The Hubble types come mostly from the Second Reference Catalog (de Vaucouleurs, de Vaucouleurs, and Corwin 1976). Particularly noisy spectra are marked with colons or double colons.

Figure 9 plots the logarithmic differences (left/sum) and (right/sum) versus sum. There is a strong indication that the percentage error is larger for dispersions less than 150 km s^{-1} ($\log \sigma = 2.18$), an effect also noted by Davies *et al.* (1987) in the Lick data. Comparison of the two slits indicates an rms error of 0.047 dex per sum for σ above this limit (based on 58 spectra with no colons). This is slightly smaller than the error of 0.057 dex found for Lick data by Davies *et al.*, but S0's and spirals tend to have higher nuclear surface brightness than ellipticals, and the spectra here thus have slightly higher signal-to-noise than those analyzed by Davies *et al.*

A comparison with dispersions from the compendium by Whitmore, McElroy, and Tonry (1985) is shown in Figure 10, where the greater scatter below 150 km s^{-1} is again evident. For the 27 objects above this limit in common, we find an offset of -0.015 ± 0.012 dex (in the sense that Lick is too low). This is consistent within the errors with the +0.010 dex offset found by Davies *et al.* Evidently *systematic errors* in the Lick measurements are small. The rms residual scatter with respect to Whitmore *et al.* is 0.061 dex, and, if equal errors are assigned to both sources, we infer an error of 0.043 dex in each. Taking account of multiple measurements, this is consistent with the slightly higher estimate of 0.047 dex *per observation* found above.

Although the errors are undoubtedly larger for dispersions below 150 km s^{-1}, this is not surprising considering that the intrinsic width of the observational point spread function of the IDS at 5000 Å is $\sigma = 260$ km s^{-1} (corresponding to a Gaussian profile of FWHM = 10 Å). Broadening of such a profile by 150 km s^{-1} corresponds to width increase of only 15%—and even less for smaller broadening. However, judging from the scatter in Figures 9–10, the S/N in the data seems adequate to return moderately useful information even for small values of σ below 150 km s^{-1}. This has been achieved in part through very careful attention to fitting the baseline, as discussed in § VI. From experience with these data (and also

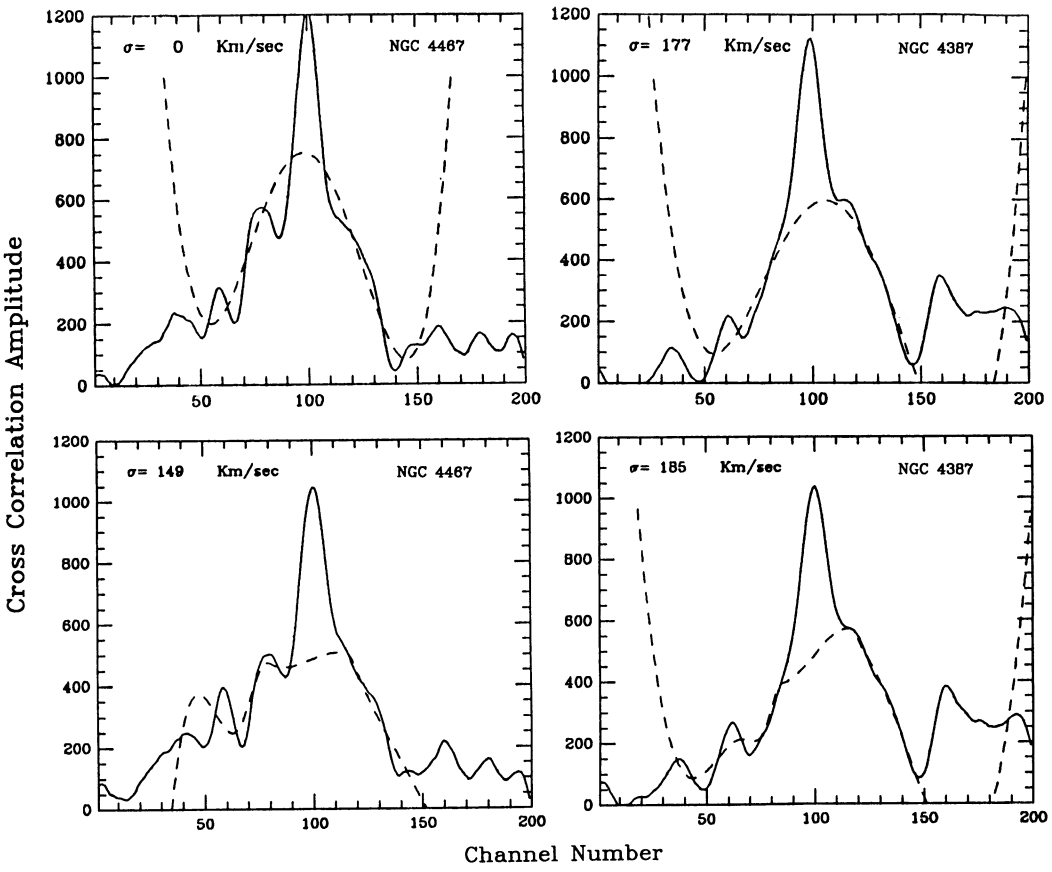

FIG. 7*b*

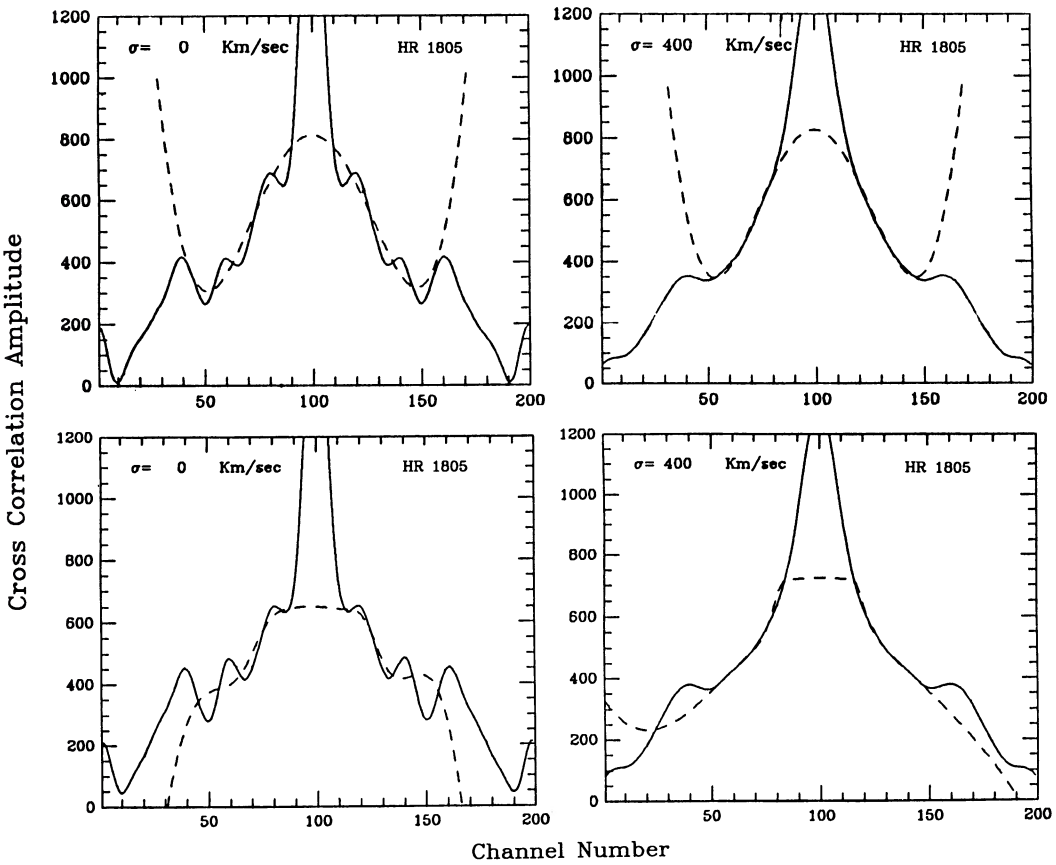

FIG. 7*c*

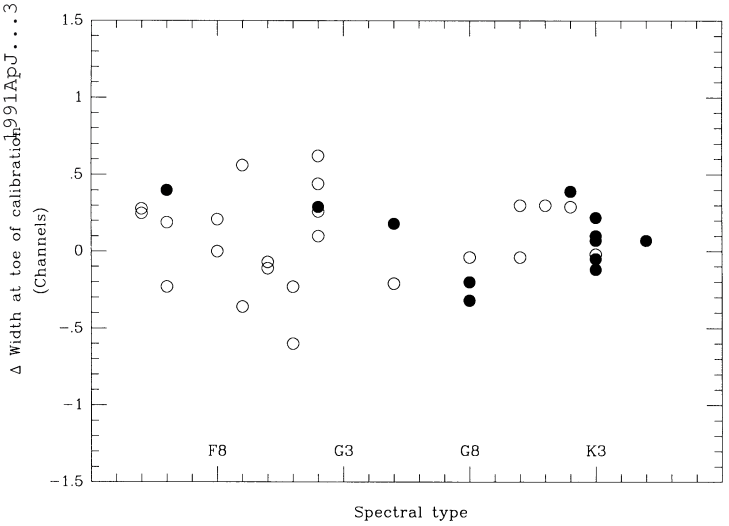

FIG. 8.—The difference between the width of the cross-correlation curve at zero broadening for various standard stars (dwarfs = *open circles*; giants = *solid dots*) and the autocorrelation of that night's K-giant template against itself. No trend is seen with spectral type or luminosity class. The slight positive offset is due to the fact that the autocorrelation of the template against itself is biased slightly too narrow due to noise.

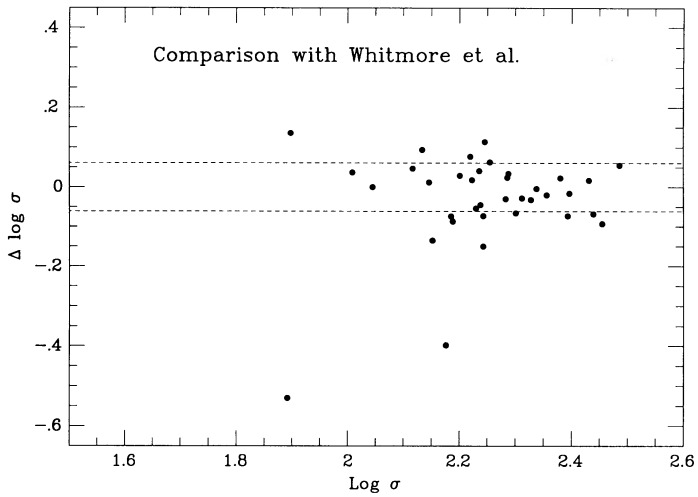

FIG. 10.—Comparison of the mean values from Table 1 with the compendium of velocity dispersions by Whitmore *et al.* (1985). The difference log (Lick/Whitmore *et al.*) is plotted versus Whitmore *et al.* Note again the larger errors below $\sigma = 150$ km s^{-1} (log $\sigma = 2.18$). The dashed lines represent $\pm 1\ \sigma$, where σ is the mutual scatter of 0.061 dex (*see text*).

with the spectra reported in Davis *et al.*, which included a large number of low-σ galaxies), we believe that the scatter in Figures 9 and 10 fairly reflects the accuracy and limits of the Lick observations.

The dispersions in Table 1 are typical of early-type galaxies and do not require much comment. The only measurement deserving special mention is the special observation of M31 under conditions of excellent seeing through a 1″ by 1″ slit (see footnote a in Table 1). This gave a dispersion of 255 km s^{-1}, much higher than the 166 km s^{-1} in Whitmore *et al.* or the values 166–198 km s^{-1} obtained here under normal seeing conditions. A rise in the central dispersion of M31 was detected in good seeing by Dressler and Richstone (1988) and by Kormendy (1988), who obtained maxima of 225 km s^{-1}. This, plus rapid rotation, was interpreted by these authors as probable evidence for a nuclear black hole. Our measurement supports this and suggests that a further increase in velocity dispersion might be visible under even better resolution, for example, with the Hubble Space Telescope.

We would like to thank Ron Markze for his assistance in reducing the velocity dispersions. This work was supported by National Science Foundation grants AST 7608258, AST 8211551, and AST 8702899.

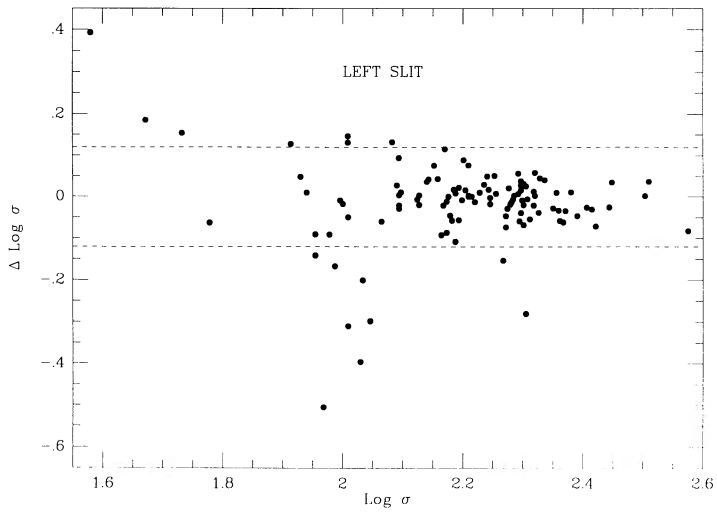

FIG. 9*a*

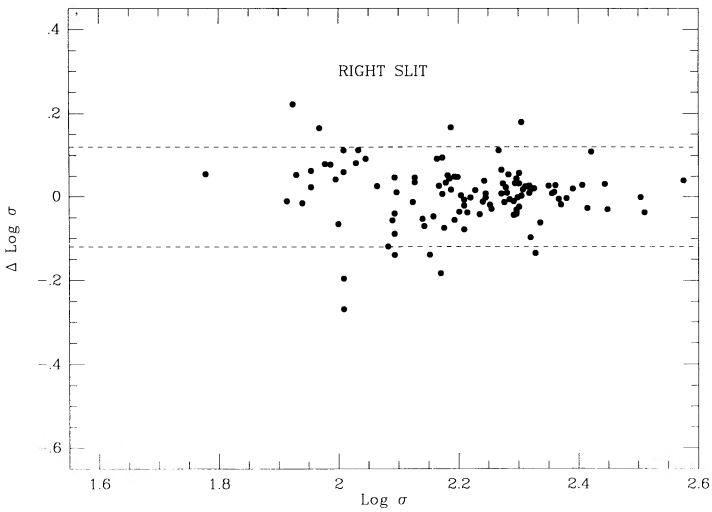

FIG. 9*b*

FIG. 9.—(*a*), (*b*)—The difference log (left/sum) and log (right/sum) for galaxies without colons in Table 1. The RMS error of the sum for galaxies above 150 km s^{-1} (log $\sigma = 2.18$) is 0.047; for galaxies below that value the errors are larger. The dashed lines show $\pm 2\ \sigma$ for each slit (for galaxies above 150 km s^{-1}).

TABLE 1

VELOCITY DISPERSIONS

Galaxy	Hubble Type	Sum	Right Slit	Left Slit	Mean
IC 1131		0	104	0	0
NGC 128	S0 P	198	219	181	198
NGC 224	SAb	196	191	199	186
		191	195	185	
		166	165	161	
		176	179	175	
		198	184	211	
		189	183	198	
NGC 224[a]	SAb	255[a]	272[a]	240[a]	255[a]
NGC 524	SA0+	281	262	304	281
NGC 598	SAcd	0	0	0	0
		0	0	34	
NGC 670	SA0	102	117	91	102
NGC 833	Sa: P	324	297	352	324
NGC 936	SB0+	208	221	198	204
		200	189	215	
NGC 1023	SB0−	208	212	214	216
		224	238	210	
NGC 1079	SAB0/a P	160	161	166	160
NGC 1291	SB0/a	162	154	162	162
NGC 1302	SB0/a	162	159	163	162
NGC 1326	SB0+	123	108	131	123
NGC 1332	S0−:sp	319	318	320	347
		376	412	311	
NGC 1375	S0:sp	55	0	0	55
NGC 1380	SA0	217	188	238	217
NGC 1380B	S0:	99	109	97	99
NGC 1638	SAB0°?	121	92	164	138
		156	137	164	
NGC 1808	SABa	152	171	133	152
NGC 2217	SB0+	209	167	239	209
NGC 2549	SA0°sp	150	126	150	150
NGC 2655	SAB0/a	153	169	159	170
		187	190	168	
NGC 2681	SAB0/a	124	101	154	111
		84:	140:	0:	
NGC 2685	SB0 P	111:	137	56	111:
NGC 2781	SAB0+	154	160	157	149
		142:	103:	169:	
NGC 2784	SA0°:	246	257	221	253
		260	244	242	
NGC 2787	SB0+	193	190	194	210
		227	231	232	
NGC 2962	SAB0+	197	212	172	197
NGC 3031	SAab	198	180	205	198
NGC 3032	SAB0°	82	80	110	82
NGC 3384	SB0−:	156	174	137	156
NGC 3414	S0 P	240	238	246	240
NGC 3489	SAB0	116	123	101	104
		97	116	66	
		100	86	96	
NGC 3626	SA0+	144	129	159	146
		149	185	122	
NGC 3665	SA0°	192	217	189	192
NGC 3817[b]		102:	65:	143:	133
		149	151	145	
NGC 3900	SA0+	154::	226::	120::	154::
NGC 3945	SB0+	174	169	195	174
NGC 4104	S0	264:	339:	224:	264:
NGC 4111	SA0	147	156	140	144
		151	163	136	
		124:	90:	125:	
NGC 4138	SA0+	134	149	135	165
		196	177	223	
NGC 4150	SA0°?	87	84	89	43
		0	97	0	
NGC 4203	SAB0−:	124	138	116	124
NGC 4262	SB0−	229	235	212	229
NGC 4270	S0	200	215	191	200
NGC 4281	S0+:sp	230	245	201	230
NGC 4324	SA0+	108	140	68	108
NGC 4350	SA0sp	179	171	201	179
NGC 4377	SA0−	169	175	173	169
NGC 4378	SAa	202::	305::	106::	202::
NGC 4382	SA0+ P	172	156	184	172
NGC 4457	SAB0/a	102	55	138	102

TABLE 1—*Continued*

Galaxy	Hubble Type	Sum	Right Slit	Left Slit	Mean
NGC 4459	SA0+	175	191	182	189
		203	211	200	
		188	202	176	
NGC 4526	SAB0°:	235	225	217	235
NGC 4570	S0sp	205	217	181	208
		212	222	194	
NGC 4578	SA0°?	60	68	52	60
NGC 4623	SB0+?sp	90	104	65	91
		93	136	29	
NGC 4694	SB0 P	85	96	95	42
		0	0	0	
NGC 4762	SB0°?sp	125	128	128	129
		124	113	118	
		139	118	153	
NGC 4866	SA0+:sp	233	230	202	233
NGC 4958	SB0?sp	164	150	164	164
NGC 5084	S0sp	198	181	216	198
NGC 5101	SB0/a	162	135	193	162
NGC 5273	SA0°	54	0	77	54
NGC 5631	SA0°	138	122	150	138
NGC 5687	S0−?	209	217	210	194
		180	168	183	
NGC 5701	SB0/a	134	145	128	120
		107	129	43	
NGC 5854	SB0+sp	148	97	193	148
NGC 6166A [c]		213::	156::	236::	200:
		187:	217:	158:	
NGC 6340	SA0/a	146	180	118	146
NGC 6359	SA0−:	190	200	182	190
NGC 6903	S0 P?	185::	239::	130::	185::
NGC 7013	SA0/a	90	95	73	90
NGC 7332	S0 Psp	95	114	77	126
		158	176	155	
NGC 7371	SA0/a:	159	146	195	159
NGC 7377	Sa0+	176	175	169	139
		102	132	50	
NGC 7457	SA0−?	0	66	0	23
		47	0	72	
NGC 7576	SA0+	38	0	94	38
NGC 7585	SA0+ P	200	228	171	201
		202	203	214	

[a] This is a special observation of M 31 under conditions of especially good seeing through a 1" by 1" aperture.
[b] S0 in MKW 10 (Morgan, Kaiser, and White 1975).
[c] Brightest embedded subnucleus in NGC 6166.

REFERENCES

Brault, J. M., and White, D. R. 1971, *Astr. Ap.*, **13**, 169.
Burstein, D., Faber, S. M., Gaskell, C. M., and Krumm, N. 1984, *Ap. J.*, **287**, 586.
Davies, L. R., Burstein, D., Dressler, A., Faber, S. M., Lynden-Bell, D., Terlevich, R. J., and Wegner, G. 1987, *Ap. J. Suppl.*, **64**, 581.
de Vaucouleurs, G., de Vaucouleurs, A., and Corwin, H. 1976, *The Second Reference Catalog of Bright Galaxies*, (Austin: University of Texas Press).
Dressler, A., and Richstone, D. O. 1988, *Ap. J.*, **324**, 701.
Faber, S. M., and Jackson, R. E. 1976, *Ap. J.*, **204**, 668.
Faber, S. M., Burstein, D., Friel, E., and Gaskell, C. M. 1985, *Ap. J. Suppl.*, **57**, 711.
Illingworth, G. 1976, *Ap. J.*, **204**, 73.
Illingworth, G., and Freeman, K. C. 1974, *Ap. J. (Letters)*, **188**, L83.
Kormendy, J. 1988, *Ap. J.*, **325**, 128.
Minkowski, R. 1962, in *Problems of Extra-Galactic Research*, ed. C. G. McVittie (New York: MacMillan), p. 112.
Morton, D. C., and Elmegreen, B. G. 1976, *Ap. J.*, **205**, 63.
Morton, D. C., and Thuan, T. X. 1973, *Ap. J.*, **180**, 705.
Richstone, D., and Sargent, W. L. W. 1972, *Ap. J.*, **176**, 91.
Robinson, L., and Wampler, E. J. 1972, *Pub. A.S.P.*, **84**, 161.
Sargent, W. L. W., Schechter, P. L., Boksenberg, A., and Shortridge, K. 1977, *Ap. J.*, **212**, 326.
Simkin, S. M. 1974, *Astr. Ap.*, **31**, 129.
Tonry, J., and Davis, M. 1979, *A.J.*, **84**, 1511.
Williams, T. B. 1976, *Ap. J.*, **209**, 716.
Whitmore, B., McElroy, D. B., and Tonry, J. 1985, *Ap. J. Suppl.*, **59**, 1.

DAVID BURSTEIN: Department of Astronomy and Physics, Arizona State University, Tempe, AZ 85287-1504

CRISTINA DALLE ORE: Center for Astrophysics, 60 Garden Street, Cambridge, MA 02138

S. M. FABER and J. JESÚS: University of California Observatories/Lick Observatory, University of California, Santa Cruz, CA 95064

ROLAND STOUGHTON: MS 34, Science Applications International Corporation, 10260 Campus Point Drive, San Diego, CA 92121